Received: 1 August 2016 | Revised: 29 November 2016 | Accepted: 19 December 2016

DOI: 10.1002/nbm.3694

WILEY NMR IN BIOMEDICINE

RESEARCH ARTICLE

Parallel transmission RF pulse design with strict temperature constraints

Cem M. Deniz[1,2,3,4,5] | Giuseppe Carluccio[1,2,3] | Christopher Collins[1,2,3,4]

[1] Center for Advanced Imaging Innovation and Research (CAI2R), New York University School of Medicine, New York, NY, USA

[2] Bernard and Irene Schwartz Center for Biomedical Imaging, Department of Radiology, New York University School of Medicine, New York, NY, USA

[3] The Sackler Institute of Graduate Biomedical Sciences, New York University School of Medicine, New York, NY, USA

[4] NYU WIRELESS, New York University Tandon School of Engineering, Brooklyn, NY, USA

[5] RF Test Labs, Inc., New York, NY, USA

Correspondence
C. M. Deniz, Department of Radiology, New York University School of Medicine, 660 1st Avenue, 4th Floor, New York, NY 10016.
Email: cemmurat.deniz@nyumc.org

Funding information
Grant/Award Numbers: NIH P41 EB017183 and NIH R01 EB011551.

RF safety in parallel transmission (pTx) is generally ensured by imposing specific absorption rate (SAR) limits during pTx RF pulse design. There is increasing interest in using temperature to ensure safety in MRI. In this work, we present a local temperature correlation matrix formalism and apply it to impose strict constraints on maximum absolute temperature in pTx RF pulse design for head and hip regions. Electromagnetic field simulations were performed on the head and hip of virtual body models. Temperature correlation matrices were calculated for four different exposure durations ranging between 6 and 24 min using simulated fields and body-specific constants. Parallel transmission RF pulses were designed using either SAR or temperature constraints, and compared with each other and unconstrained RF pulse design in terms of excitation fidelity and safety. The use of temperature correlation matrices resulted in better excitation fidelity compared with the use of SAR in parallel transmission RF pulse design (for the 6 min exposure period, 8.8% versus 21.0% for the head and 28.0% versus 32.2% for the hip region). As RF exposure duration increases (from 6 min to 24 min), the benefit of using temperature correlation matrices on RF pulse design diminishes. However, the safety of the subject is always guaranteed (the maximum temperature was equal to 39°C). This trend was observed in both head and hip regions, where the perfusion rates are very different.

KEYWORDS

parallel transmission, RF pulse design, temperature constraints, temperature correlation matrices

1 | INTRODUCTION

RF fields are used in MRI to excite nuclei to a state where they can produce a detectable signal. The interaction between RF electromagnetic (EM) fields and conducting body tissues generates electrical currents, which cause tissue heating. Heat absorbed by biological tissues can lead to significant changes in the underlying temperature distribution.[1–8] For this reason, in applications involving RF exposure, it becomes crucial to predict temperature change in order to avoid unsafe temperatures that may cause tissue damage. The International Electrotechnical Commission (IEC) has provided guidelines to guarantee the safety of the patient during MRI.[9] Limits are imposed primarily on the maximum temperature reached in the human body. Due to the complexity of measuring temperature *in situ*, the maximum RF power absorbed per unit mass (specific absorption rate; SAR) is used as a secondary surrogate metric for safety. Equivalent SAR is computed to comply with the temperature recommendations of IEC using simple models. Typically, SAR, either averaged over a 10 g tissue volume (10 g SAR) or averaged over a whole exposure volume (global SAR), is the quantity most used to monitor safety, even though temperature has a more direct relationship to tissue damage and is accepted as a safety metric internationally.[9]

Several RF pulse design strategies[10–14] have been proposed for incorporating 10 g and/or global SAR into pulse design, aiming to achieve safe operation of parallel transmit systems by controlling SAR while achieving design goals, such as inhomogeneity mitigation and SAR minimization. SAR based safety control of multichannel transmit systems during RF pulse design has been made tractable by using virtual observation points (VOPs)[15] in EM field simulations to reduce the number of monitored locations with predefined SAR overestimation. For transmit arrays, where the field distribution can change through time, utilizing VOPs dramatically speeds up optimization and design processes of RF pulses with SAR constraints.[12,14] In addition

Abbreviations used: B_1^+, transmit RF magnetic field; EM, electromagnetic; NRMSE, normalized root mean square error; pTx, parallel transmission; SAR, specific absorption rate; *S*-parameter, scattering parameter; VOP, virtual observation point

to the methods using VOP compression, another fast RF pulse design method[16] has become available to eliminate the need for SAR overestimation by using SAR at all voxels without compression, aiming at better SAR control during pulse design.

Temperature has attracted interest as a safety metric for parallel transmit pulse design instead of SAR. For example, one group suggested that it would be possible to find the worst-case local temperature increase[17] with use of temperature matrices as developed for use in hyperthermia,[18–20] but did not implement their use for that purpose. Moreover, a parallel transmission RF pulse design approach has been proposed for a 3D time-of-flight sequence imposing strict temperature constraints by updating strict SAR constraints based on temperature simulations at each iteration.[21] It was shown that the use of strict temperature constraints enabled the use of high-SAR RF pulses while keeping the local temperature within defined IEC safety limits by relaxing SAR limits. Recently, RF pulse design approaches aiming to overcome B_1^+ inhomogeneity while explicitly constraining the temperature rise have been demonstrated using EM field simulations involving a head coil loaded with a human subject[22–24] and local temperature correlation matrices.[18,20]

In this work, we present a local temperature correlation matrix formalism for parallel transmission, which is applied to identify the maximum temperature inside the subject due to RF exposure for a specific heating time. Local temperature correlation matrices are incorporated into RF pulse design, aiming to satisfy limits on local maximum absolute temperature during pulse design. In previous work,[22–24] local temperature matrices were used to constrain only temperature increase. Our aim in this study is to use the maximum absolute temperature as a strict safety constraint in RF pulse design using local temperature correlation matrices. Fast parallel transmit RF pulse design is achieved by using the VOP approach to reduce the number of calculated local temperature correlation matrices from EM field simulations. In order to investigate the effect of perfusion characteristics of the region of interest on RF pulse design with strict maximum temperature constraints, simulations were performed on the head (with brain having relatively high perfusion rates) and the hip (containing only tissues with relatively low perfusion rates) using two different local multichannel transmit arrays. RF pulse designs for multiple RF exposure durations (ranging from 6 min to 24 min with 6 min intervals) were performed in order to investigate the characteristics of using maximum temperature constraints rather than SAR constraints in different parts of the body. A preliminary description of this work has been presented previously.[22,25]

2 | THEORY

Let us suppose we have a series of M RF pulses in one interval T_R (Figure 1), and for each of these pulses there is a combination of amplitudes and phases of the N channels of a transmit array. These M RF pulses can hypothetically have different durations and amplitudes within the same sequence with short T_R. This combination associated with the mth pulse is stored in the complex vector $\boldsymbol{v_m} = [\boldsymbol{v}_{1,m} \ldots \boldsymbol{v}_{N,m}]^T$. For each RF pulse and for each voxel of the inspected subject, $\mathbf{r}$, it is [illegible] local electric field correlation matrix $\boldsymbol{\Lambda}$

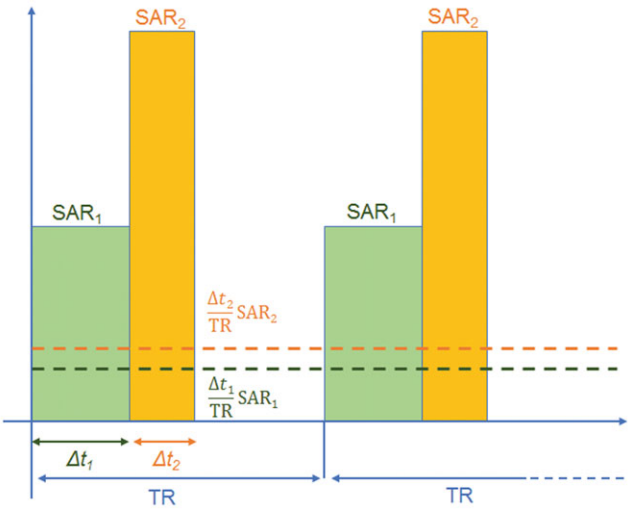

FIGURE 1 Schematic diagram of two different hard RF pulses in the time interval T_R (solid bars), and the relative levels associated with them averaged over each T_R (dashed lines)

$$\boldsymbol{\Lambda}(\mathbf{r}) = \begin{bmatrix} \frac{\sigma(\mathbf{r})}{\rho(\mathbf{r})}\mathbf{E}_1^*(\mathbf{r})\mathbf{E}_1(\mathbf{r}) & \cdots & \frac{\sigma(\mathbf{r})}{\rho(\mathbf{r})}\mathbf{E}_N^*(\mathbf{r})\mathbf{E}_1(\mathbf{r}) \\ \vdots & \ddots & \vdots \\ \frac{\sigma(\mathbf{r})}{\rho(\mathbf{r})}\mathbf{E}_1^*(\mathbf{r})\mathbf{E}_N(\mathbf{r}) & \cdots & \frac{\sigma(\mathbf{r})}{\rho(\mathbf{r})}\mathbf{E}_N^*(\mathbf{r})\mathbf{E}_N(\mathbf{r}) \end{bmatrix} \quad (1)$$

where σ is the electrical conductivity, ρ is the material density, $\mathbf{E}_n$ is the electric field generated by the nth channel when driven with unit voltage and * denotes the complex conjugate transpose.

The definition of the matrix $\boldsymbol{\Lambda}$ allows the computation of the SAR as a result of the mth pulse in each location $\mathbf{r}$ by multiplying

$$\begin{aligned} \mathrm{SAR}_m(\mathbf{r}) &= \boldsymbol{v_m^*}\boldsymbol{\Lambda}(\mathbf{r})\boldsymbol{v_m} \\ &= v_{1,m}^*\Lambda_{11}(\mathbf{r})v_{1,m} + v_{1,m}^*\Lambda_{12}(\mathbf{r})v_{2,m} + \ldots + v_{N,m}^*\Lambda_{NN}(\mathbf{r})v_{N,m} \end{aligned} \quad (2)$$

SAR absorption induces a temperature increase inside the sample, which can be computed with a well-known bioheat equation[26]

$$\rho(\mathbf{r})c(\mathbf{r})\frac{\partial T(\mathbf{r})}{\partial t} = \nabla\cdot(k\nabla T(\mathbf{r})) - W(\mathbf{r})\rho_{\mathrm{bl}}c_{\mathrm{bl}}(T(\mathbf{r}) - T_{\mathrm{bl}}) + Q(\mathbf{r}) + \rho(\mathbf{r})\mathrm{SAR}(\mathbf{r}) \quad (3)$$

where ρ is the material density, c is the heat capacity, k is the heat conductivity, W is a blood perfusion related parameter,[27,28] Q is the heat generated by metabolism, the subscript bl indicates blood and T_{bl} is the blood temperature.

For short T_R, the temperature increase depends mainly on the average value of SAR over the time interval T_R.[29] Incorporating SAR associated with all M pulses using Equation 2 in Equation 3 yields

$$\begin{aligned} \rho(\mathbf{r})c(\mathbf{r})\frac{\partial T(\mathbf{r})}{\partial t} &= \nabla\cdot(k\nabla T(\mathbf{r})) - W(\mathbf{r})\rho_{\mathrm{bl}}c_{\mathrm{bl}}(T(\mathbf{r}) - T_{\mathrm{bl}}) + Q(\mathbf{r}) \\ &\quad + \rho(\mathbf{r})\left(\frac{\Delta t_1}{T_R}\mathrm{SAR}_1(\mathbf{r}) + \frac{\Delta t_2}{T_R}\mathrm{SAR}_2(\mathbf{r}) + \ldots + \frac{\Delta t_M}{T_R}\mathrm{SAR}_M(\mathbf{r})\right) \end{aligned} \quad (4)$$

where Δt_m is the pulse length defined on the mth hard RF subpulse. Since Equation 4 is linear, assuming (most importantly) that perfusion does not change with temperature, it is possible to focus on the

contribution from each single generic pulse separately within short T_R. Defining T_0 as the equilibrium temperature or the temperature distribution prior to RF excitation, and T_{SARm} as the temperature increase due to RF power absorption of the mth pulse, the total temperature can be expressed as a linear combination of individual temperature increase contributions $T = T_0 + \sum_{m=1}^{M} T_{SARm}$ Using the linearity of Equation 4, it is possible to find independent relationships to determine T_0 and each T_{SARm}.

$$\rho(r)c(r)\frac{\partial T_0(r)}{\partial t} = \nabla\cdot(k\nabla T_0(r)) - W(r)\rho_{bl}c_{bl}(T_0(r) - T_{bl}) + Q(r) \quad (5)$$

$$\begin{aligned}\rho(r)c(r)\frac{\partial T_{SARm}(r)}{\partial t} &= \nabla\cdot(k\nabla T_{SARm}(r)) - W(r)\rho_{bl}c_{bl}T_{SARm} \\ &\quad + \rho(r)\frac{\Delta t_m}{T_R}\mathrm{SAR}_m(r).\end{aligned} \quad (6)$$

Substituting Equation 2 into Equation 6 we find

$$\begin{aligned}\rho(r)c(r)\frac{\partial T_{SARm}(r)}{\partial t} &= \nabla\cdot(k\nabla T_{SARm}(r)) - W(r)\rho_{bl}c_{bl}T_{SARm} \\ &\quad + \rho(r)\frac{\Delta t_m}{T_R}v^*_{1,m}\Lambda_{11}(r)v_{1,m} \\ &\quad + \rho(r)\frac{\Delta t_m}{T_R}v^*_{1,m}\Lambda_{12}(r)v_{2,m} + \ldots \\ &\quad + \rho(r)\frac{\Delta t_m}{T_R}v^*_{N,m}\Lambda_{NN}(r)v_{N,m}\end{aligned} \quad (7)$$

For a given heating time t_{end}, and for the superposition of the effects in Equation 3, it is possible to write

$$\begin{aligned}T_{SARm}(r) &= \frac{\Delta t_m}{T_R}v^*_{1,m}T_{11}(r)v_{1,m} + \frac{\Delta t_m}{T_R}v^*_{1,m}T_{12}(r)v_{2,m} + \ldots \\ &\quad + \frac{\Delta t_m}{T_R}v^*_{N,m}T_{NN}(r)v_{N,m} \\ &= \frac{\Delta t_m}{T_R}\mathbf{v}^*_{\boldsymbol{m}}\mathbf{T}_{\mathrm{increase}}(r)\mathbf{v}_{\boldsymbol{m}}\end{aligned} \quad (8)$$

where each value $T_{ij}(r)$ of the temperature correlation matrix, $\mathbf{T}_{\mathrm{increase}}$, is a solution of the equation

$$\rho(r)c(r)\frac{\partial T_{ij}(r)}{\partial t} = \nabla\cdot\left(k\nabla T_{ij}(r)\right) - W(r)\rho_{bl}c_{bl}T_{ij} + \rho(r)\Lambda_{ij}(r) \quad (9)$$

calculated numerically from $t = 0$ to $t = t_{end}$. Once all the values T_{ij} are computed with Equation 9, the number of locations where the matrix $\mathbf{T}_{\mathrm{increase}}$ is evaluated can be reduced with the use of the VOP compression used for the SAR.[15] In fact, Equation 2 and Equation 8 reveal that $\mathbf{T}_{\mathrm{increase}}$ has the same structure as the $\boldsymbol{\Lambda}$ matrix, in that they are both positive definite and Hermitian. The temperature increase T_{inc} from an applied RF pulse can be finally computed with the sum

$$T_{\mathrm{inc}}(\mathbf{r}) = \sum_{m=1}^{M}\frac{\Delta t_m}{T_R}\mathbf{v}^*_{\boldsymbol{m}}\mathbf{T}_{\mathrm{increase}}(\mathbf{r})\mathbf{v}_{\boldsymbol{m}} \quad (10)$$

such that the absolute temperature becomes

$$T(\mathbf{r}) = T_0(\mathbf{r}) + \sum_{m=1}^{M}\frac{\Delta t_m}{T_R}\mathbf{v}^*_{\boldsymbol{m}}\mathbf{T}_{\mathrm{increase}}(\mathbf{r})\mathbf{v}_{\boldsymbol{m}} \quad (11)$$

This matrix formalism allows very fast computation of the temperature during RF pulse design or other purposes, such as RF safety monitoring using $\mathbf{T}_{\mathrm{increase}}$ matrices for temperature prediction.

3 | METHODS

3.1 | Electromagnetic field simulations for head and hip transmit array

EM field simulations were performed to obtain electric and magnetic field distributions induced by a head-sized eight element 7 T transmit array containing the numerical head model including shoulders with 5 mm isometric resolution[30] (Figure 2). A commercial finite-difference time domain solver (XFdtd 6.6, Remcom, State College, PA, USA) was used for simulations. Individual coils were designed as copper stripline transmitters with dimensions of 30 × 2 cm^2 on a 36 cm diameter shield. Individual coil electric and magnetic field distributions within the HUGO head model were exported from a number of voxels R = 48 566.

In addition to the simulations performed on the head array, we used experimentally validated EM field simulations of a hip transmit array[31,32] in order to investigate the effect of RF pulse design with temperature based safety metrics in regions with no tissues as highly perfused as brain. EM field simulation of an eight channel hip array and torso phantom setup was performed with CST Microwave Studio (CST 2014, Darmstadt, Germany). Each simulated coil was tuned to

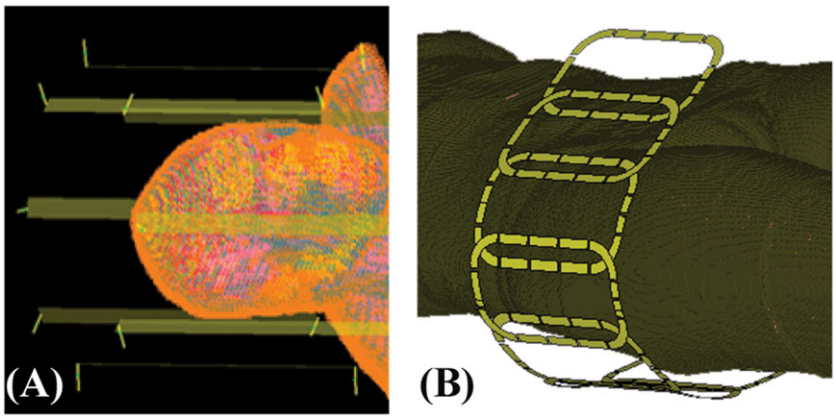

FIGURE 2 Simulation geometries. A, Eight channel head transmit array with the head model (shield not shown). B, Eight channel hip [illegible] Fila virtual body model

297.2 MHz and matched using co-simulation[33,34] based scattering-parameter (*S*-parameter) analysis by aligning with the bench measurements of *S*-parameters in the actual coil. 125 million mesh cells with edge lengths ranging from 0.05 mm to 28 mm were used in the EM field calculations. The loss and phase delay between the RF coil plug and individual coils (including T/R switches, coaxial cables, and cable traps) were measured and applied to the EM field simulations. The simulated electric and magnetic fields of each coil were compared with the measured MR field[35] and temperature.[32,36] Using the validated hip transmit array, EM field simulations of the Ella body model[37] (1 mm isometric resolution) was performed. Individual coil electric and magnetic field distributions within the model were exported from a number of voxels R = 10 958 786.

At each spatial location $\mathbf{r}$, temperature correlation matrices, $\mathbf{T}_{\text{increase}}$, of a multi-channel RF transmit system were calculated from EM field simulations. The elements of local electric field correlation matrices, $\mathbf{\Lambda}$, were used as source terms in Equation 9 for a specific imaging sequence length, t_{end} = 6 min (SAR averaging duration recommended by IEC[9]), of a gradient-echo based sequence with T_R = 9 ms. Simulations performed for analyzing the effect of scan durations on SAR and temperature constraints have the same duty cycle. Voxel specific constants in Equation 9, such as metabolic rate, density, heat capacity, and electrical properties at 297.2 MHz, were obtained from the literature.[38] Initial temperature distributions, $T_0(\mathbf{r})$, were obtained by calculating the steady state temperature distribution of the body using an ambient air temperature of 23°C. Temperature simulations were performed using a finite-difference approximation based temperature simulator.[39] The equilibrium temperature computed with no SAR applied until the average temperature distribution of two consecutive time steps was less than 10^{-21}°C.

The concept of VOPs[15] was incorporated to replace complete $\mathbf{T}_{\text{increase}}$ matrices with a smaller number of constructed matrices with VOPs $\mathbf{Z}^j$, j = 1, ..., N (N, the number of temperature VOPs, is much less than R, the number of voxels in the EM field simulation), designed to provide an acceptable maximum 5% overestimation of the worst-case temperature increase per unit RF excitation. The overestimation percentage is chosen such that the number of VOPs is small enough to accelerate the RF pulse design without causing too much overestimation of the SAR and temperature, which will reduce performance. When calculating the VOPs for 10 s average SAR, for every voxel $\mathbf{r}$, $\mathbf{\Lambda}(\mathbf{r})$ matrices were averaged over a spherically defined 10 g mass, and thus yielded $\mathbf{\Lambda}^{10\,g}$ matrices. $\mathbf{\Lambda}^{10\,g}$ matrices were used to calculate SAR VOPs, $\mathbf{Z}_k^{10\,g}$ k = 1, ..., K (K, the number of 10 g SAR VOPs, is much less than R), with maximum 5% overestimation of the worst-case 10 g SAR, and were used to guarantee 10 g SAR limits during constrained RF pulse design. This smaller number of VOPs enable fast calculation of parallel transmits RF pulses. A spherical volume, rather than cubic, was chosen because thermal conduction from one location in an unconfined homogeneous region occurs equally in all directions making a spherical volume naturally more relevant for safety assurance.

3.2 | RF pulse design

The temperature contribution summation of each hard pulse $\boldsymbol{v}_m$ of [illegible]10 can be written as a quadratic function of input RF pulse $\boldsymbol{v}_{\text{full}} = \left[\boldsymbol{v}_1^{\mathrm{T}} \ldots \boldsymbol{v}_M^{\mathrm{T}}\right]^{\mathrm{T}}$, where M is the number of hard RF subpulses, which is the concatenation of coil RF pulse waveforms, $\boldsymbol{v}_m$:

$$T_{\text{inc}}(\mathbf{r}) = \boldsymbol{v}_{\text{full}}^{*}\mathbf{T}_{\text{full}}(\mathbf{r})\boldsymbol{v}_{\text{full}}, \text{ where } \mathbf{T}_{\text{full}} = \frac{\Delta t}{T_R}\begin{bmatrix} \mathbf{T}_{\text{increase}} & & 0 \\ & \ddots & \\ 0 & & \mathbf{T}_{\text{increase}} \end{bmatrix} \tag{12}$$

Using Equation 12, temperature increase resulting from any RF pulse excitation can be calculated easily for each location inside the sample and T_R. One way of integrating temperature increase prediction capability into RF pulse design is to use the following quadratic inequalities for a given temperature increase limit T_{lim}:

$$\boldsymbol{v}_{\text{full}}^{*}\mathbf{T}_{\text{full}}(\mathbf{r})\boldsymbol{v}_{\text{full}} \leq T_{\text{lim}} \quad \forall \mathbf{r} \tag{13}$$

Similarly, maximum tissue temperature limits as specified by the standards[9] can be incorporated into the RF pulse design by closely tracking the tissue temperature before RF exposure, $T_0(\mathbf{r})$:

$$T_0(\mathbf{r}) + \boldsymbol{v}_{\text{full}}^{*}\mathbf{T}_{\text{full}}(\mathbf{r})\boldsymbol{v}_{\text{full}} \leq 39°\text{C} \quad \forall \mathbf{r} \tag{14}$$

Using the small-tip-angle approximation[40] and discretizing in N_m time and N_s spatial positions similarly to Reference [41], transverse magnetization after RF excitation can be written in a matrix form by defining a full system matrix $\mathbf{A}_{\text{full}} = [\mathbf{A}_1 \ \cdots \ \mathbf{A}_N]$ in which the $\mathbf{A}_l$ are $N_s \times N_m$ system matrices with elements $a_{ij} = \mathrm{i}\gamma\Delta t M_0(\mathbf{r}_i) S^{(l)}(\mathbf{r}_i) \mathrm{e}^{\mathrm{i}\gamma\Delta B_0(\mathbf{r}_i)(t_j - T)} \mathrm{e}^{\mathrm{i}\mathbf{r}_i \cdot \mathbf{k}(t_j)}$ where γ is the gyromagnetic ratio, $M_0(\mathbf{r})$ is the equilibrium magnetization, $S^{(l)}(\mathbf{r})$ is the B_1^+ sensitivity patterns of the transmit coils, $\Delta B_0(\mathbf{r})$ is the local off-resonance field map, $\mathbf{k}(t)$ is the excitation k-space trajectory, N is the number of transmit coils and m is the hard RF subpulse index. Using the matrix form of the system matrix and temperature increase limits, the parallel excitation RF pulse design problem with strict temperature increase constraints can be written as

$$\hat{\boldsymbol{v}}_{\text{full}} = \underset{\boldsymbol{v}_{\text{full}}}{\text{argmin}} \ \|\mathbf{A}_{\text{full}}\boldsymbol{v}_{\text{full}} - \mathbf{m}_{\text{des}}\|_2^2 \quad \text{subject to } \boldsymbol{v}_{\text{full}}^{*}\mathbf{Z}_{\text{full}}^{j}\boldsymbol{v}_{\text{full}} \leq T_{\text{lim}} \text{ OR } T_{0,j} + \boldsymbol{v}_{\text{full}}^{*}\mathbf{Z}_{\text{full}}^{j}\boldsymbol{v}_{\text{full}} \leq 39°\text{C} \quad \forall j \tag{15}$$

where $\mathbf{m}_{\text{des}}$ is the desired magnetization profile from RF excitation, and $\mathbf{Z}_{\text{full}}^{j}$ are the block diagonal matrices that contain temperature increase information, temperature VOPs, to be used in conjunction with $\boldsymbol{v}_{\text{full}}$. $T_{0,j}$ is the maximum initial temperature located within the cluster of the jth VOP. RF pulses designed with temperature constraints ("temperature constrained") were compared with RF pulses designed with 10 g averaged SAR constraints ("10 g SAR constrained") as well as RF pulses designed without any constraints ("unconstrained"). All RF pulses were designed with maximum absolute temperature constraints by solving Equation 15. In order to study the effect of scan durations on SAR and temperature constraints, all three types of RF pulse were designed for multiple RF exposure durations (varying between 6 min

and 24 min) by using the corresponding temperature correlation matrices that are calculated based on the RF exposure duration. In Equation 15, error minimization term with respect to the desired target profile is defined as a quadratic cost functional of the desired RF pulse and system matrix. Temperature constraints in the optimization problem are defined as quadratic functions of the desired RF pulse. Since local temperature correlation, $\mathbf{T}_{\text{increase}}$, matrices are positive definite and defined constraints are quadratic functions, the optimization problem can be solved inside the convex search space defined by quadratic constraints. The optimization problem in Equation 15 can be solved by using a range of efficient strategies for convex optimization. Similar to previous RF pulse design approaches,[11,14] a least-squares projection strategy was employed for solving the optimization problem, using, specifically, a Lanczos algorithm with Gram-Schmidt re-orthogonalization steps.[42] Using the Lanczos algorithm, the number of basis vectors were reduced to 50 with exact temperature constraints enabling fast and memory efficient calculation of the solution to the optimization problem. This reduced basis convex optimization problem was solved efficiently using the SeDuMi v1.2.1 solver[43] interfaced with YALMIP.[44]

3.3 | Head transmit array

In the present study, a constant rate spiral-in excitation *k*-space trajectory was used in a gradient-echo based sequence with T_R = 9 ms with the following parameters: duration = 3.1 ms, excitation resolution = 2.5 mm, sampling interval = 10 μs, maximum gradient slew rate = 150 mT/m/s and gradient amplitude = 40 mT/m. Parallel excitation RF pulses for uniform 30° excitation in a 2D rectangular region on the center axial slice were designed by solving Equation 15 with maximum temperature constraints. $\mathbf{T}_{\text{increase}}$ matrices were replaced by 252 temperature VOPs, **Z**, in RF pulse design enabling a predefined maximum 5% overestimation of the worst-case temperature increase per unit RF excitation in each subvolume. The local temperature limit on the constraint was defined as 39°C. Similarly, VOP compression on $\mathbf{\Lambda}^{10\,g}$ matrices resulted in 364 10 g SAR VOPs, $\mathbf{Z}^{10\,g}$. The local 10 g SAR limit was defined as 10 W/kg.

3.4 | Hip transmit array

For the hip transmit array, a constant rate spiral-in excitation *k*-space trajectory was used in a gradient-echo based sequence with T_R = 9 ms with the following parameters: duration = 2.2 ms, sampling interval = 10 μs, maximum gradient slew rate = 150 mT/m/s and gradient amplitude = 40 mT/m. Parallel excitation RF pulses for uniform 25° excitation in a 2D disk on the hip region were designed by solving Equation 15 with maximum temperature constraints. $\mathbf{T}_{\text{increase}}$ matrices were replaced by 932 temperature VOPs, **Z** (maximum 5% overestimation of the worst case). The local temperature limit on the constraint was defined as 39°C. Similarly, VOP compression on $\mathbf{\Lambda}^{10\,g}$ matrices resulted in 1010 10 g SAR VOPs, $\mathbf{Z}^{10\,g}$. The local 10 g SAR limit was defined as 10 W/kg.

4 | RESULTS

4.1 | Head transmit array

Desired 2D excitation profile and simulated axial flip angle maps resulting from RF pulses designed with different constraints are shown in Figure 3. Defined constraints were always satisfied by the convex optimization and remaining degrees of freedom were used to minimize the excitation error. Temperature constrained design results in lower excitation errors compared with 10 g SAR constrained design, while satisfying current MR safety standards.[9] The maximum local spatial average 10 g SAR was 18.0 W/kg for the temperature constrained design, 10 W/kg for the 10 g SAR constrained design and 20.9 W/kg for the unconstrained design (Table 1).

Figure 4 shows temperature and 10 g SAR resulting from RF pulses designed with temperature constraints on one slice of the head. As depicted by the black squares, the maximum temperature and 10 g SAR are located in different regions within the slice.

TABLE 1 Maximum temperature, maximum 1 g SAR, maximum 10 g SAR, and NRMSE resulting from RF pulses designed with various strict constraints for the head model in head transmit array for 6 min of RF exposure. (NRMSE is defined as the flip angle root mean square error between the achieved and the targeted profile divided by the root mean square of the target excitation flip angle profile)

Pulse design type	Unconstrained	10 g SAR constrained	Temperature constrained
Maximum local temperature (°C)	39.3	38.4	39.0
Maximum 1 g SAR (W/kg)	35.1	17.6	30.5
Maximum 10 g SAR (W/kg)	20.9	10.0	18.0
NRMSE (%)	7.8	21.0	8.8

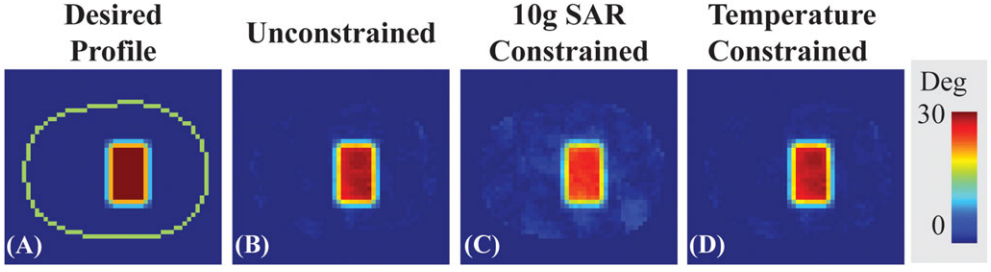

FIGURE 3 Desired profile on an axial slice of the head model (A), and flip angle distributions of RF pulses designed without constraints B, with 10 g SAR constraints (C), and with temperature constraints (D), for 6 min of RF exposure. The periphery of the head is indicated with a green line

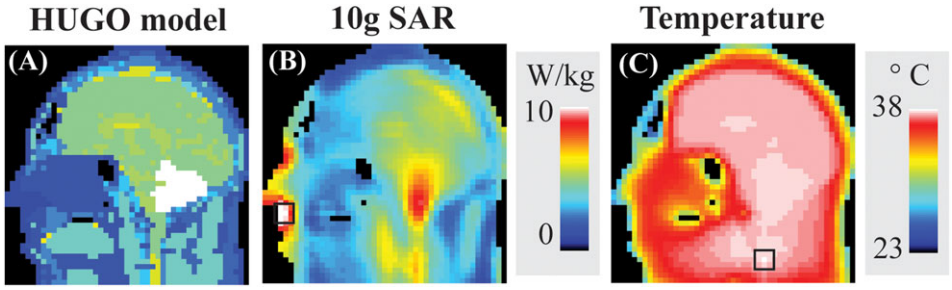

FIGURE 4 A, Material distribution of the head model. B,C, 10 g SAR B, and temperature (C), resulting from temperature constrained RF pulse designs. Maximum 10 g SAR and temperature in the slice are indicated by the black squares located in different regions of the head

4.2 | Hip transmit array

Figure 5 shows desired 2D excitation profile and simulated axial flip angle maps resulting from RF pulses designed with different constraints. Similar to the head transmit array simulation results, defined constraints were always satisfied by the convex optimization and remaining degrees of freedom were used to minimize the excitation error. The maximum local spatial average 10 g SAR was 20.7 W/kg for the temperature constrained design, 10 W/kg for 10 g SAR constrained design and 30.1 W/kg for the unconstrained design (Table 2). The maximum local temperature limit of 39°C was exceeded by around 1°C with the RF pulse design having no constraints. The temperature constrained design result in around 15% lower error in excitation profile compared with the SAR constrained design, while satisfying the current MR safety standard.[9]

Figure 6 shows temperature and 10 g SAR resulting from RF pulses designed with temperature constraints in the hip region. Similar to head simulations, as depicted by the black squares, the maximum temperature and 10 g SAR are located in different regions for hip simulations within the slice.

4.3 | RF exposure duration

Figure 7 shows the maximum temperature, maximum SAR, and flip angle normalized root mean square error (NRMSE) resulting from RF pulses designed for different RF exposure durations in both head and hip regions. In both regions, designed unconstrained RF pulses, as expected, resulted in constant NRMSE and the maximum SAR for all exposure durations. On the other hand, the maximum temperature increased with exposure duration reaching 40.4°C and 43.7°C at the end of 24 min of imaging for head and hip regions, respectively. In the 10 g SAR constrained design, the maximum temperature increased from 38.4°C to 38.9°C and 38.2°C to 39.3°C for head and hip regions, respectively, while NRMSE and the maximum SAR were constant as the exposure duration is increased. In contrast to the trends observed for unconstrained and 10 g SAR constrained RF pulse designs, in

TABLE 2 Maximum temperature, maximum 1 g SAR, maximum 10 g SAR, and NRMSE resulting from RF pulses designed with various strict constraints for Ella virtual body model in hip transmit array for 6 min of RF exposure

Pulse design type	Unconstrained	10 g SAR constrained	Temperature constrained
Maximum local temperature (°C)	39.9	38.1	39.0
Maximum 1 g SAR (W/kg)	75.9	19.9	46.9
Maximum 10 g SAR (W/kg)	30.1	10.0	20.7
NRMSE (%)	27.0	32.2	27.5

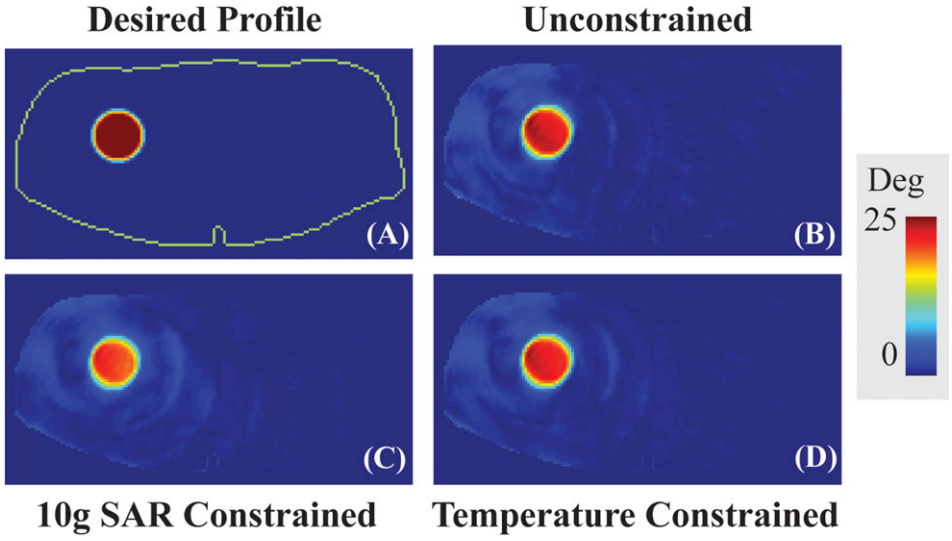

FIGURE 5 Desired profile (in red) on an axial slice through the Ella virtual model A, and Bloch simulation resulting from RF pulses designed without safety constraints B, with 10 g SAR constraints C, and with temperature constraints (D), for 6 min of RF exposure. The periphery of the body is [illegible] line (A)

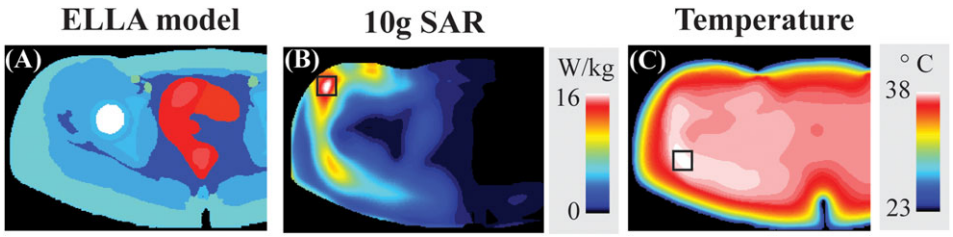

FIGURE 6 A, Material distribution of the Ella virtual body model. B,C, Multiple intensity projections of 10 g SAR (B), and temperature (C), results from temperature constrained RF pulse designs. Maximum temperature and 10 g SAR are indicated by the black squares, which are located in different regions of the head. The right-hand side of the simulations, which was not covered by the hip array, was cropped for visualization

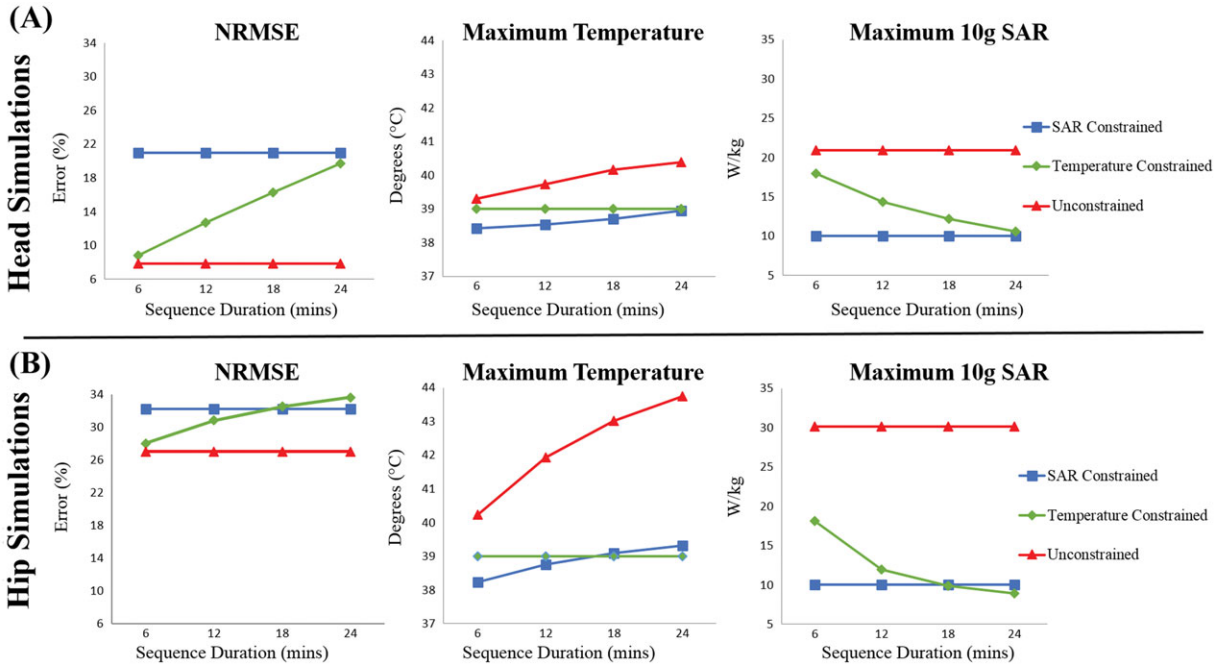

FIGURE 7 The effect of RF exposure duration in RF pulse design using temperature correlation matrices. NRMSE, maximum temperature, and maximum 10 g SAR resulting from RF pulses designed with various strict constraints for head (A), and hip (B), regions

temperature constrained design for the hip region, the NRMSE increased (from 28.0% to 33.6%) and the maximum SAR decreased (from 18.2 W/kg to 8.9 W/kg) as RF exposure duration is increased (from 6 min to 24 min). In the head, the NRMSE increased (from 8.8% to 19.7%) and the maximum SAR decreased (from 18.0 W/kg to 10.6 W/kg) as the RF exposure duration is increased (from 6 min to 24 min). In both head and hip regions, the maximum temperature remained constant at 39°C as RF exposure duration changed. In order to meet strict temperature safety requirements, some compromise in NRMSE was required during temperature constrained RF pulse design. For sequence durations up to 18 min and above 24 min, lower NRMSE was obtained using strict temperature constraints compared with SAR constraints in the hip region and head region, respectively. For both head and hip regions, higher benefits of using temperature constraints are obtained for shorter sequence durations.

5 | DISCUSSION

In this work, we demonstrated the concept of using a local tempera- ix, $\mathbf{T}_{\text{increase}}$, calculated from local electric field correlation matrices using EM field and temperature simulations of human models, for safety assurance in pulse design. Calculated $\mathbf{T}_{\text{increase}}$ matrices are compressed using VOPs and used in design of parallel RF transmission pulses with strict maximum temperature constraints. The use of temperature correlation matrices in RF pulse design resulted in increased excitation fidelity and provided a more relevant safety metric compared with SAR.

Calculation of $\mathbf{T}_{\text{increase}}$ matrices needs to be performed prior to RF pulse calculations with predefined t_{end} and T_R. To the extent that the $\mathbf{T}_{\text{increase}}$ matrices match the true tissue characteristics *in vivo*, using predefined temperature limits in a parallel transmission RF pulse design will ensure a safe MR scan. The proposed RF design process with $\mathbf{T}_{\text{increase}}$ matrices is fully capable of enforcing different temperature increase limits for different parts of the body, e.g. in the eyes, by predefining VOP clusters in those regions. In addition to the constraints involving temperature predictions for a specific t_{end}, system related constraints such as individual channel forward and reflected peak and average power can be incorporated into the RF pulse optimization problem in Equation 15 using calibrated power correlation matrices.[14]

In this study, we incorporated limits on the absolute temperature into the RF pulse design by adding the maximum predetermined

temperature before RF excitation to each VOP cluster in the constraints as defined in Equation 11. Similarly, local temperature increase limits[22,24] can easily be incorporated into the RF pulse design. Methods for fast tracking body temperature during an MR examination for safety purposes have also been proposed.[29] In the future, further development of those approaches will enable the integration of temperature correlation matrices into MR scanners for closely monitoring safe operation and proactively managing RF pulse design.

We demonstrate that using temperature correlation matrices for parallel transmission RF pulses constraining maximum absolute temperature is beneficial in both head and hip regions. Our results are in agreement with previous investigations obtained in the head using constraints on temperature increase,[22–24] indicating that better excitation profiles can be achieved with temperature constraints than with SAR constraints. We also investigated the hip region, which has lower perfusion rates than those present in the brain. Regardless of the perfusion characteristics differences, our results indicate that using temperature correlation matrices enables lower excitation errors, especially for shorter RF exposure durations, and still ensures patient safety, remaining below the maximum temperature limits. Only for the hip at the longest exposure duration studied does the SAR constrained pulse provide a slightly better NRMSE than the temperature constrained one, and it does so at a cost of temperatures slightly exceeding 39°C. As the RF exposure duration is increased, the benefit of using temperature correlation matrices diminishes for both head and hip regions. However, safe operation (the maximum temperature always below 39°C) is always guaranteed by using temperature correlation matrices, with the expense of increased excitation error, while using strict SAR constraints may result in exposure conditions where the maximum local temperature exceeds 39°C. It is also important to note that continuous exposures to a single SAR distribution and level (single sequence) lasting up to 24 min are increasingly rare in practice. Rather, shorter sequences with different SAR levels are applied in series, often with breaks in between them during which temperature will progress towards the baseline. Thus, we believe that the results for exposure periods shorter than 24 min are more relevant in practice. Related to this, the methods discussed here are intended for pulse design more than for safety assurance of an actual patient examination, which can be accomplished very rapidly even with consideration of multiple thermo-regulatory effects and the increase of whole-body temperature.[29]

The comparison with different parts of the body reveals the benefit of using temperature correlation matrices up to a specific exposure duration to be region independent. Also, while it has been shown that the perfusion can be a function of local tissue temperature, here the perfusion of tissues was kept constant with respect to temperature. This may result in reduced RF pulse design performance; however, it provides an additional safety factor. Computational demands for performing high resolution simulations and actual resolutions of the virtual body models limit the use of very fine resolutions. In this study, EM field simulations were performed using two different virtual body models with resolutions of 1 mm isometric for the hip region and 5 mm isometric for the head. While 5 mm may seem coarse, in a study of the effects of model resolution on whole-head and 1 g averaged SAR, no notable difference was seen between resolutions of 5 mm isometric and 2 × 2 × 2.5 mm^3.[45]

In simulations, we incorporated the proposed local temperature correlation matrices and RF pulse design approach to short-T_R SAR limited 3D GRE based hip microarchitecture scans at high field strengths.[46] This type of sequence is expected to benefit from the proposed RF pulse design with temperature constraints as opposed to the existing SAR constraints.[21] In the future, we plan to use this approach for *in vivo* studies targeting safe operation and minimal excitation error. Current practice for ensuring subject safety of parallel RF excitations using SAR as a metric relies on estimating field distributions from simulations of the RF array with multiple virtual subjects covering the population of interest and their positions with respect to the array,[47–50] and making sure that the worst-case 10 g SAR distributions are below what has been traditionally obtained from quadrature excitations.[9] Similar approaches for estimating field distributions and validated thermal properties of the virtual subjects could enable calculation of the temperature correlation matrices for specific RF exposure duration. Thus, temperature correlation matrices for multiple exposure durations could be calculated once prior to RF pulse design and used later for RF pulse design as long as temperature prior to RF exposure is tracked accurately.[29]

Although computation of SAR induced temperature rather than SAR alone can be seen to add a layer of complexity and uncertainty to assurance of safety, the result is more relevant to the actual risk to the subject and it is always possible to ensure safety with conservative methods designed to ensure an overestimate of temperatures compared with what is expected *in vivo*. The method implemented here, for example, does not allow for a thermoregulatory increase in perfusion rates at locations of high temperature, as occurs *in vivo*. This approach has been seen to overestimate temperature increases observed *in vivo*, even while giving very good estimates of temperature in a phantom.[8] Another related study showed that very dramatic increases in perfusion with temperature were required to avoid overestimation of temperatures observed *in vivo*.[51] Thus, in this work use of temperature rather than SAR to maximize safety in pulse design allows for lower constraints in many cases despite the temperature predictions being conservative, which is a clear advantage to use of temperature. The existing limits on SAR are designed to be conservative, and our results indicate that in many cases they are conservative to the point of being more restrictive than use of the temperature limits. Although the method used here for pulse design does not allow for increase in the whole-body core temperature and thus the temperature of incoming blood at each location, after the pulse design is completed fast methods of temperature prediction allowing for core body temperature to increase with consideration of whole-body SAR and many other heat transfer mechanisms such as respiration, perspiration, and convection[29,52] can be used to ensure safety while also allowing for conservative increases in local perfusion to avoid overly restrictive safety assurance measures. Other methods for computing temperature increase considering additional factors have also been proposed to consider additional factors,[28] including discrete vasculature to a fairly high resolution.[53] In general, however, they are nonlinear and are not suitable for fast pulse design.

6 | CONCLUSIONS

We have demonstrated that temperature correlation matrices can facilitate integration of limits on maximum absolute temperature into parallel transmission RF pulse design. Because temperature is ultimately more relevant to subject safety than SAR, we hope this will inspire further advances in making temperature a routine consideration for ensuring RF safety in MRI.

ACKNOWLEDGEMENTS

We thank Leeor Alon and Martijn A. Cloos for initial discussions on the temperature correlation matrices, and Daniel K. Sodickson for his support throughout the study.

This work was supported in part by NIH R01 EB011551 and was performed under the rubric of the Center for Advanced Imaging Innovation and Research (CAI^{2}R, www.cai2r.net), an NIBIB Biomedical Technology Resource Center (NIH P41 EB017183).

REFERENCES

1. Barber BJ, Schaefer DJ, Gordon CJ, Zawieja DC, Hecker J. Thermal effects of MR imaging: worst-case studies on sheep. *Am J Roentgenol*. 1990;155(5):1105–1110.
2. Shrivastava D, Hanson T, Kulesa J, DelaBarre L, Iaizzo P, Vaughan JT. Radio frequency heating at 9.4 T (400.2 MHz): in vivo thermoregulatory temperature response in swine. *Magn Reson Med*. 2009;62(4):888–895.
3. Shrivastava D, Hanson T, Schlentz R, et al. Radiofrequency heating at 9.4 T: in vivo temperature measurement results in swine. *Magn Reson Med*. 2008;59(1):73–78.
4. Shrivastava D, Hanson T, Kulesa J, Tian J, Adriany G, Vaughan JT. Radiofrequency heating in porcine models with a "large" 32 cm internal diameter, 7 T (296 MHz) head coil. *Magn Reson Med*. 2011;66(1):255–263.
5. Nadobny J, Klopfleisch R, Brinker G, Stoltenburg-Didinger G. Experimental investigation and histopathological identification of acute thermal damage in skeletal porcine muscle in relation to whole-body SAR, maximum temperature, and CEM43 °C due to RF irradiation in an MR body coil of birdcage type at 123 MHz. *Int J Hyperthermia*. 2015;31(4):409–420.
6. Shrivastava D, Utecht L, Tian J, Hughes J, Vaughan JT. In vivo radiofrequency heating in swine in a 3 T (123.2-MHz) birdcage whole body coil. *Magn Reson Med*. 2014;72(4):1141–1150.
7. Shuman WP, Haynor DR, Guy AW, Wesbey GE, Schaefer DJ, Moss AA. Superficial- and deep-tissue temperature increases in anesthetized dogs during exposure to high specific absorption rates in a 1.5-T MR imager. *Radiology*. 1988;167(2):551–554.
8. Oh S, Ryu Y-C, Carluccio G, Sica CT, Collins CM. Measurement of SAR-induced temperature increase in a phantom and in vivo with comparison to numerical simulation. *Magn Reson Med*. 2014;71(5):1923–1931.
9. International Electrotechnical Commission. *Medical Electrical Equipment—Part 2-33: Particular Requirements for the Basic Safety and Essential Performance of Magnetic Resonance Equipment for Medical Diagnosis*. IEC 60601–2-33 ed3.0; 2010.
10. Zhu Y. Parallel excitation with an array of transmit coils. *Magn Reson Med*. 2004;51(4):775–784.
11. Brunner DO, Pruessmann KP. Optimal design of multiple-channel RF pulses under strict power and SAR constraints. *Magn Reson Med*. 2010;63(5):1280–1291.
12. Lee J, Gebhardt M, Wald LL, Adalsteinsson E. Local SAR in parallel transmission pulse design. *Magn Reson Med*. 2012;67(6):1566–1578.
13. Guérin B, Setsompop K, Ye H, Poser BA, Stenger AV, Wald LL. Design [illegible]sion pulses for simultaneous multislice with explicit control for peak power and local specific absorption rate. *Magn Reson Med*. 2014;73(5):1946–1953.
14. Deniz CM, Alon L, Brown R, Zhu Y. Subject- and resource-specific monitoring and proactive management of parallel radiofrequency transmission. *Magn Reson Med*. 2015;76:20–31.
15. Eichfelder G, Gebhardt M. Local specific absorption rate control for parallel transmission by virtual observation points. *Magn Reson Med*. 2011;66(5):1468–1476.
16. Pendse M, Rutt B. IMPULSE: a generalized and scalable algorithm for joint design of minimum SAR parallel transmit RF pulses. Presented at: ISMRM 23rd Annual Meeting and Exhibition; Toronto; 2015:543.
17. Neufeld E, Gosselin MC, Murbach M, Christ A, Cabot E, Kuster N. Analysis of the local worst-case SAR exposure caused by an MRI multi-transmit body coil in anatomical models of the human body. *Phys Med Biol*. 2011;56(15):4649
18. Das SK, Clegg ST, Samulski TV. Computational techniques for fast hyperthermia temperature optimization. *Med Phys*. 1999;26(2):319–328.
19. Das SK, Jones EA, Samulski TV. A method of MRI-based thermal modelling for a RF phased array. *Int J Hyperthermia*. 2001;17(6):465–482.
20. Köhler T, Maass P, Wust P, Seebass M. A fast algorithm to find optimal controls of multiantenna applicators in regional hyperthermia. *Phys Med Biol*. 2001;46(9):2503
21. Boulant N, Massire A, Amadon A, Vignaud A. Radiofrequency pulse design in parallel transmission under strict temperature constraints. *Magn Reson Med*. 2014;72(3):679–688.
22. Deniz CM, Carluccio G, Sodickson DK, Collins CM. Non-iterative parallel transmission RF pulse design with strict temperature constraints. Presented at: ISMRM 23rd Annual Meeting and Exhibition; Toronto; 2015:549.
23. Boulant N, Xiaoping W, Adriany G, Schmitter S, Ugurbil K, Van de Moortele PF. Direct control of the temperature rise in parallel transmission via temperature virtual observation points: simulations at 10.5 T. Presented at: ISMRM 23rd Annual Meeting and Exhibition; Toronto; 2015:548.
24. Boulant N, Wu X, Adriany G, Schmitter S, Uğurbil K, Van de Moortele P-F. Direct control of the temperature rise in parallel transmission by means of temperature virtual observation points: simulations at 10.5 tesla. *Magn Reson Med*. 2015;75(1):249–256.
25. Carluccio G, Deniz CM, Collins CM. An approach to temperature-based virtual observation points for safety assurance and pulse design. Presented at: ISMRM 23rd Annual Meeting and Exhibition; Toronto; 2015:3220.
26. Bernardi P, Cavagnaro M, Pisa S, Piuzzi E. Specific absorption rate and temperature elevation in a subject exposed in the far-field of radio-frequency sources operating in the 10-900-MHz range. *IEEE Trans Biomed Eng*. 2003;50(3):295–304.
27. Roemer RB, Dutton AW. A generic tissue convective energy balance equation: part I—theory and derivation. *J Biomech Eng*. 1998;120(3):395–404.
28. Shrivastava D, Vaughan JT. A generic bioheat transfer thermal model for a perfused tissue. *J Biomech Eng*. 2009;131(7):074506–074506.
29. Carluccio G, Bruno M, Collins CM. Predicting long-term temperature increase for time-dependent SAR levels with a single short-term temperature response. *Magn Reson Med*. 2015;75(5):2195–2203.
30. Collins CM, Smith MB. Signal-to-noise ratio and absorbed power as functions of main magnetic field strength, and definition of "90 degrees" RF pulse for the head in the birdcage coil. *Magn Reson Med*. 2001;45(4):684–691.
31. Deniz CM, Brown R, Alon L, et al. Multi-channel array safety simulations validated with field and temperature measurements. Presented at: ISMRM-ESMRMB Joint Annual Meeting; Milan; 2014:4929.
32. Deniz CM, Brown R, de Zwart JA, Collins CM, Sodickson DK. Multi-channel array safety using least squares fitting based MR thermometry.

Presented at: ISMRM Workshop on Safety in MRI: Guidelines, Rationale & Challenges; 2014; Washington, DC.

33. Paska J, Froehlich J, Brunner DO, Pruessmann KP, Vahldieck R. Field superposition method for RF coil design. In: *17th Annual ISMRM Scientific Meeting and Exhibition 2009*. Berkeley, CA: ISMRM; 2009:3619.
34. Kozlov M, Turner R. Fast MRI coil analysis based on 3-D electromagnetic and RF circuit co-simulation. *J Magn Reson*. 2009;200(1):147–152.
35. Van den Berg CAT, Bartels LW, van den Bergen B, et al. The use of MR B_1^+ imaging for validation of FDTD electromagnetic simulations of human anatomies. *Phys Med Biol*. 2006;51(19):4735.
36. Cline H, Mallozzi R, Li Z, McKinnon G, Barber W. Radiofrequency power deposition utilizing thermal imaging. *Magn Reson Med*. 2004;51(6):1129–1137.
37. Gosselin MC, Neufeld E, Moser H, et al. Development of a new generation of high-resolution anatomical models for medical device evaluation: the Virtual Population 3.0. *Phys Med Biol*. 2014;59(18):5287.
38. Hasgall PA, Di Gennaro F, Baumgartner C, et al. IT'IS Database for thermal and electromagnetic parameters of biological tissues, Version 2.6, September 01st, 2015. doi: 10.13099/ViP-Database-V2.6
39. Collins CM, Liu W, Wang J, et al. Temperature and SAR calculations for a human head within volume and surface coils at 64 and 300 MHz. *J Magn Reson Imaging*. 2004;19(5):650–656.
40. Pauly J, Nishimura D, Macovski A. A k-space analysis of small-tip-angle excitation. *J Magn Reson*. 1989;81(1):43–56.
41. Grissom W, Yip CY, Zhang Z, Stenger VA, Fessler JA, Noll DC. Spatial domain method for the design of RF pulses in multicoil parallel excitation. *Magn Reson Med*. 2006;56(3):620–629.
42. Golub GH, Loan CFV. *Matrix Computations*. 3rd ed. Baltimore, MD, USA: Johns Hopkins University Press; 1996.
43. Sturm J. Primal-Dual Interior Point Approach to Semidefinite Programming. Amsterdam: Tinbergen Institute; 1997.
44. Löfberg J. YALMIP: a toolbox for modeling and optimization in MATLAB. In: *2004 IEEE International Symposium on Computer Aided Control Systems Design*; IEEE; 2005. doi: 10.1109/CACSD.2004.1393890
45. Collins CM, Smith MB. Spatial resolution of numerical models of man and calculated specific absorption rate using the FDTD method: a study at 64 MHz in a magnetic resonance imaging coil. *J Magn Reson Imaging*. 2003;18(3):383–388.
46. Chang G, Deniz CM, Honig S, et al. MRI of the hip at 7 T: feasibility of bone microarchitecture, high-resolution cartilage, and clinical imaging. *J Magn Reson Imaging*. 2014;39(6):1384–1393.
47. Graesslin I, Homann H, Biederer S, et al. A specific absorption rate prediction concept for parallel transmission MR. *Magn Reson Med*. 2012;68(5):1664–1674.
48. Homann H, Börnert P, Eggers H, Nehrke K, Dössel O, Graesslin I. Toward individualized SAR models and in vivo validation. *Magn Reson Med*. 2011;66(6):1767–1776.
49. Voigt T, Homann H, Katscher U, Doessel O. Patient-individual local SAR determination: in vivo measurements and numerical validation. *Magn Reson Med*. 2012;68(4):1117–1126.
50. de Greef M, Ipek O, Raaijmakers AJE, Crezee J, van den Berg CAT. Specific absorption rate intersubject variability in 7 T parallel transmit MRI of the head. *Magn Reson Med*. 2013;69(5):1476–1485.
51. Murbach M, Neufeld E, Capstick M, et al. Thermal tissue damage model analyzed for different whole-body SAR and scan durations for standard MR body coils. *Magn Reson Med*. 2014;71(1):421–431.
52. Carluccio G, Erricolo D, Oh S, Collins CM. An approach to rapid calculation of temperature change in tissue using spatial filters to approximate effects of thermal conduction. *IEEE Trans Biomed Eng*. 2013;60(6):1735–1741.
53. van Lier ALHMW, Kotte ANTJ, Raaymakers BW, Lagendijk JJW, van den Berg CAT. Radiofrequency heating induced by 7 T head MRI: thermal assessment using discrete vasculature or Pennes' bioheat equation. *J Magn Reson Imaging*. 2012;35(4):795–803.

How to cite this article: Deniz CM, Carluccio G, Collins, C. Parallel transmission RF pulse design with strict temperature constraints. *NMR in Biomedicine*. 2017;30:e3694. https://doi.org/10.1002/nbm.3694